A Joint Experimental and LES Characterization of the Liquid Fuel Spray in a Swirl Injector

Guillaume Vignat, Preethi Rajendram Soundararajan, D. Durox, Aymeric Vié, Antoine Renaud, Sébastien Candel

GT2020-14935

A Joint Experimental and LES Characterization of the Liquid Fuel Spray in a Swirl Injector

Guillaume Vignat*, Preethi Rajendram Soundararajan, Daniel Durox, Aymeric Vié, Antoine Renaud, Sébastien Candel
EM2C Laboratory, CentraleSupelec and CNRS, Université Paris-Saclay, 91192 Gif sur Yvette, France
Email: guillaume.vignat@centralesupelec.fr

ABSTRACT

The quality of liquid fuel spray injection determines to a large extent the steady state performance and dynamics of gas turbine and aero-engine combustors. The present investigation is focused on the detailed characterization of the liquid fuel spray in a single sector test rig targeted at aero-engine applications. The liquid fuel (heptane) is injected in a hollow cone spray pattern by a simplex atomizer and the injector comprises a radial swirler. Two features of the droplet distribution that are less commonly found in the technical literature are identified. First, the distributions of mean droplet diameters exhibit non-axisymmetric patterns, a lack of symmetry that is investigated for three types of swirlers differing by their swirl number and/or head loss. Second, it is found that the size-conditioned velocity distributions feature a single wide peak for small droplets and become bimodal for the largest droplets, with a first peak at low velocities, and a second one at higher velocities. The spray behavior analysis is complemented by making use of Large Eddy Simulations with Lagrangian Particle Tracking. Droplet injection is achieved with a model in which the initial size and velocity distributions are specified from experimental data in the atomizer near field. The initial spray interacts with the lateral injector surface and requires a droplet-wall interaction model accounting for the existence of a liquid film. Simulations do not retrieve the lack of rotational symmetry that is found experimentally indicating that this is not linked to the nature of the swirling flow. This is also consistent with further experiments with a different atomizer confirming that this is due to imperfections in the initial atomizer geometry. Another result is that certain swirler designs appear to be more robust to these atomizer imperfections. Simulations accounting for the liquid film yield a bimodal distribution for the droplets' axial velocity distribution which would not be obtained without this model indicating that it is important to represent the droplet-wall interaction, a feature that is not commonly found in the literature.

*Address all correspondence to this author.

INTRODUCTION

Liquid-fueled aero-engine injectors have to handle a wide range of fuel flow rate from engine idle to full power conditions (typically 1:40) while ensuring good atomization in order to maintain combustor performance levels, in terms of pollutant emissions and operability (ignition, blow out, combustion instabilities...). To this end, many larger engines use several atomizers, or even several injectors, one of which, dubbed "pilot", is designed to handle lower flow rates and ensure reliable operation under low power settings [1]. Pressure-swirl atomizers are often used for that purpose as they give access to the required performances by generating a spray of fine droplets in a hollow cone pattern with a large angle and a homogeneous circumferential liquid distribution even under low fuel pressure and flow rates [2].

The general objective of the present article is to investigate the complex interaction taking place inside the injector between the swirling flow, the droplet cloud produced by the pressure atomizer and the injector geometry. This question is examined by combining detailed experiments and simulations. On the experimental side attention is first focused on the impact of the injector design on the circumferential droplet size distribution. The velocity distribution is measured and its features are interpreted using Large Eddy Simulation (LES).

At this stage it is worth reviewing the literature dealing with these various issues. Early characterizations of pressure-swirl atomizers are reviewed by Lefebvre [3]. Much of the work was focused on obtaining correlations between injector geometrical dimensions and performance such as discharge coefficients, cone angle and overall droplet diameter. As atomizers are integrated inside injectors, interactions between the air flow and the spray must be considered. This is accomplished for example by Rajamanickam & Basu [4] who study the interactions between the hollow cone liquid sheet formed by a simplex atomizer and a swirling air flow by systematically varying the air flow rate to investigate different flow regimes. Time resolved measurements show that the dominant mechanism for sheet break-up and primary atomization is driven by surface tension effects when the momentum of the liquid is large compared to that of the air. At higher air flows, the motion of the liquid is strongly

coupled with that of the air leading to flapping and catastrophic break-up of the liquid sheet by vortices in the air flow. The angle of the spray also increases with increasing air flow rate, a result also reported in [5] where the spray angle of a simplex atomizer is shown to increase when the air flow rate and swirl number of the surrounding air coflow are augmented. The dynamics of the disperse phase is investigated for example in [6] where particle dispersion takes place in a jet after a sudden expansion. Adding a swirling motion can lead to segregation depending on droplet size and associated Stokes number, and constitutes the working principle of cyclonic separation [7, 8]. Detailed characterization of droplet size and velocity in laboratory scale aero-engine-type combustion chamber have been made possible by advances in laser diagnostics, in particular by the development of the Phase Doppler Anemometer (PDA). An early application of this instrument by McDonnell et al. [9] showed its potential for laboratory characterization of sprays formed by aero-engine injectors. More recently, PDA has been used by Lecourt et al. [10] to fully characterize an aeronautical injector in non-reactive and reactive conditions and provide data that was then used to initiate numerical simulations [11–13]. These studies explored Eulerian and Lagrangian particle tracking approaches to model spray combustion. One lesson learned from these investigations is that a complex interaction takes place between the spray and the Precessing Vortex Core (PVC). This helicoidal coherent vortical structure that is commonly found in strongly swirling flows is also present in aeronautical injectors. This interaction subsequently perturbs the flame. Recent experiments by Renaud et al. [14] on spray-PVC interaction indicate that the PVC attaches at the tip of the atomizer, and produces a periodic disturbance of the fuel supply. Although the PVC vanishes at the injector outlet, the perturbation on the spray still influences the flame. A more detailed, joint experimental and numerical study on the interaction between a spray formed by a prefilming atomizer and a PVC was carried out by Keller et al. [15]. They compared several numerical simulation approaches and note that contrary to Unsteady Reynolds Averaged Navier Stokes (URANS), Large Eddy Simulation (LES) is better suited to predict interactions between droplets and vortical structures, leading to an improved modeling of fuel-air mixing. Their simulations also feature spray clustering: the large droplets gather and form a helical shaped volume of higher liquid loading and equivalence ratio, in phase with the PVC, somewhat at variance with Franzelli et al. [13] who find fuel loading perturbations that are delayed with respect to the PVC.

In the area of combustion dynamics, the response of droplets and of the fuel atomizer itself to acoustic perturbations is also found to play a key role in the flame response. Cold flow and spray response to acoustic perturbations of a swirl spray injector examined experimentally and with LES in [16] indicate that a slow convective wave of fuel loading is formed. This is attributed to the modulation of the droplet transport by the air flow, and to the modulation of the atomization process in the air-blast atomizer. Kim et al. [17] used LES in a similar cold flow study. Eckstein et al. [18] studied a self-excited oscillation in a single sector, laboratory scale, kerosene fueled aeronautical burner. They observe a modulation in droplet diameter being released by their injector and note that subsequent modulation on evaporation and droplet acceleration delays may play a key role in the dynamics of their flame. The joint experimental and numerical (LES) investigation [19], carried out on a high pressure, kerosene fueled test rig, underline the importance of the delay introduced by droplet evaporation on the thermoacoustic feedback loop. Finally, perhaps the best demonstration of the impact of liquid fuel injection properties on combustion instabilities is provided by Lee et al. [20], who use an actively controlled Nanomiser™to vary the fuel droplet size of their injector, allowing them to move from a stable to an unstable combustion regime of operation.

The present analysis is motivated by observations of combustion dynamical phenomena in an annular combustor "MICCA-Spray", an atmospheric test rig at EM2C laboratory used to investigate ignition and azimuthally coupled combustion dynamics. This system has been more recently converted to allow liquid fuel injection in order to be more representative of a small helicopter engine combustor [22, 23]. To better understand flame dynamics in this rig, it is necessary to take a closer look at fuel injection in this configuration and obtain information that may apply more generally to swirl injectors comprising a pressure atomizer.

The aim of this article is to present detailed measurements of cold flow spray that are necessary inputs to high fidelity simulations. These data are obtained on a single sector featuring a central injector "SICCA-Spray" (a sister test rig to "MICCA-Spray"). This configuration will first be introduced, along with the design of the injector and the diagnostic tools that have been employed. Several swirlers are used to assess the impact of swirler design and in particular that of the swirl number on the circumferential distribution of fuel. The spray is then characterized using laser tomography and Phase Doppler Anemometry. These data are then combined with Large Eddy Simulations. This is accomplished by first presenting the numerical setup, validating calculations with experimental results and finally gathering insights from the LES and experimental measurements to discuss key aspects of the injected spray.

EXPERIMENTAL SETUP AND INJECTOR DESIGN

The "SICCA-Spray" atmospheric test rig (Fig. 1) comprises a plenum fed with compressed air. In the present unconfined cold flow experiments, the mixture of air and fuel created by the injector is dumped to the atmosphere. The air flow rate is controlled by two Bronkhorst EL-Flow mass flow controllers (relative accuracy of 1%). Liquid heptane is injected through the atomizer, and its flow rate is measured by a Bronkhorst CORI-Flow controller, with a relative accuracy of 0.5%. For clarity, we will designate in this paper the atomizer as the element through which the liquid fuel forms a spray (orange in Fig. 1), while "injector" is used to designate the whole system placed between the air plenum and the combustion chamber through which air is channeled, mixed

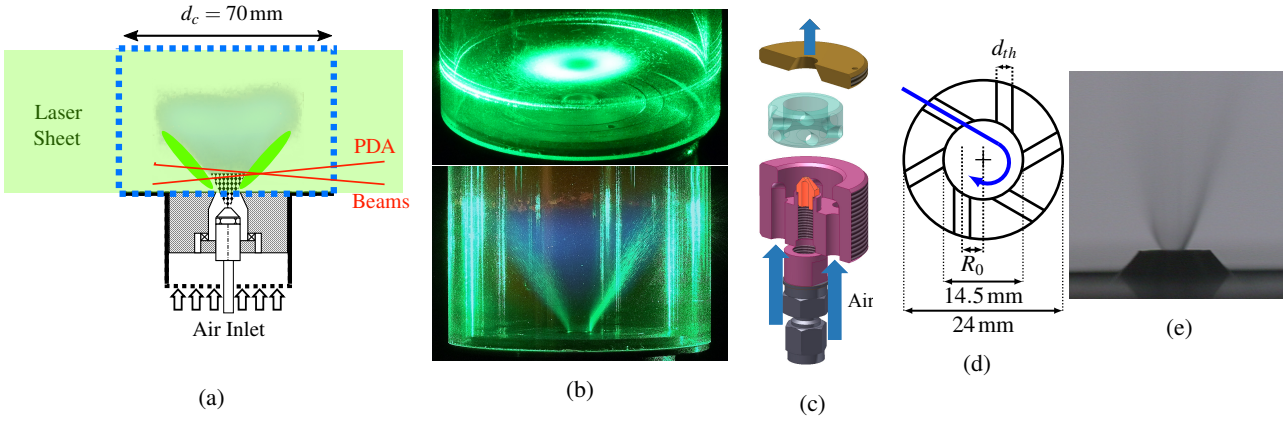

Fig. 1: From left to right: **(*a*)** Schematic view of the "SICCA-Spray" test rig. The air plenum is not shown (see however [21] for more details). Approximate position of the laser sheet (green), the field of view of the camera (blue dotted square) and the laser beams of the PDA system (red) are shown. **(*b*)** True color photographs of "SICCA-Spray" under reactive conditions. The "M-shaped" flame is visible in blue. A Nd:YaG laser sheet is used to obtain a droplet tomography in two directions, illustrating the hollow cone shape of the spray. **(*c*)** Exploded view of the injector and its components. In purple, the main body, in orange the liquid fuel atomizer, in translucide teal the tangential air swirler and in gold the injector outlet, which is flush mounted in the chamber backplane. Adapted from [22]. **(*d*)** Schematic view of the swirler seen from above indicating the main dimensions of this component. **(*e*)** Shadowgraph visualization of a typical spray near the tip of the atomizer.

with fuel and prepared to stabilize combustion. The injector consists in an axial channel that is fed with air from the plenum and conveys the flow to a tangential hole swirler. The flow is set in rotation and starts mixing with the fuel before being exhausted in the chamber or in the atmosphere through first a 5 mm long conical section followed by a 1 mm long cylinder. The outlet diameter of the injector is $d_{inj} = 8\,\text{mm}$. The atomizer (orange in Fig. 1(c), part number IJ2582-0-00) is manufactured by ADIndustries Hydraulics (formerly MicroMécanique Pyrénéenne, Oloron-Sainte-Marie, France) and is a pressure-swirl, simplex design with a manufacturer specified flow number of $\text{FN} = 0.261\text{h}^{-1}\text{bar}^{-0.5}$ and an atomizer final orifice radius of $r_{at} = 40\,\mu\text{m}$. Following the final orifice, the atomizer features a diverging cup with an included half angle of 59 deg and a final diameter of 1.5 mm. The tip of the atomizer is set 5.6 mm in recess from the dump plane.

The spray is characterized with a Dantec Dynamics FlowExplorer Fiber PDA 2 component Phase Doppler Anemometer that simultaneously measures fuel droplet diameters and velocities in a small probe volume ($0.14\,\text{mm} \times 0.14\,\text{mm} \times 0.23\,\text{mm}$). Spray tomographies are obtained with a 600 mW Nd:YaG continuous laser operating at 532 nm wavelength. A Panasonic Lumix FZ38 camera is used for acquiring images.

SWIRLER DESIGN IMPACT ON FUEL SPRAY PATTERN

It is first interesting to examine the impact of the swirler design on the fuel spray circumferential pattern. A homogeneous circumferential distribution of the spray is usually desired to ensure symmetry of the flame and avoid formation of hot spots which may reduce the service life of the high pressure distributor and increase pollutant emissions [2]. This characteristic of the spray is however seldom studied. McDonnell et al. [9] performed such a study on three methanol-fueled air-blast atomizer used in a helicopter engine, and showed the advantage of PDA against the more traditional patternator for such a study. However, only manufacturing dispersion was considered.

In the present section, the spray characteristics are examined for six variants of the injection system. Two different atomizers are used: the first designated as AG was observed to form a circumferentially homogeneous spray. The second, AD, was damaged by repetitive electrical discharges during plasma assisted combustion experiments. Its circumferential spray pattern is skewed.

The sprays formed with the two atomizers are characterized for three different swirlers, dubbed 707, 712 and 716, designed by varying the diameter d_{th} and the excentricity R_0 of the tangential holes (see Fig. 1(d)). Note that swirler 716 is the one being used in a recent investigation of azimuthal combustion instabilities [22]. The operating point considered in what follows corresponds to a heptane mass flow rate of $500\,\text{g}\,\text{h}^{-1}$ and an air flow rate of $2.3\,\text{g}\,\text{s}^{-1}$.

The aerodynamic characteristics of the different swirlers are summed up in Tab. 1. The head loss ΔP of the air flow between the upstream side of the injector and the atmosphere is measured using a Kimo MP111 differential pressure gauge with a 1% relative accuracy. Laser Doppler Velocimetry (LDV) yields flow velocities in the absence of fuel injection. In these experiments, the air is seeded with silicon oil droplets with a Mean Diameter of around 2.6 µm [24]. Results are shown in Fig. 2. Swirler 707 and 712 are designed to have identical velocity profiles downstream of the injector,

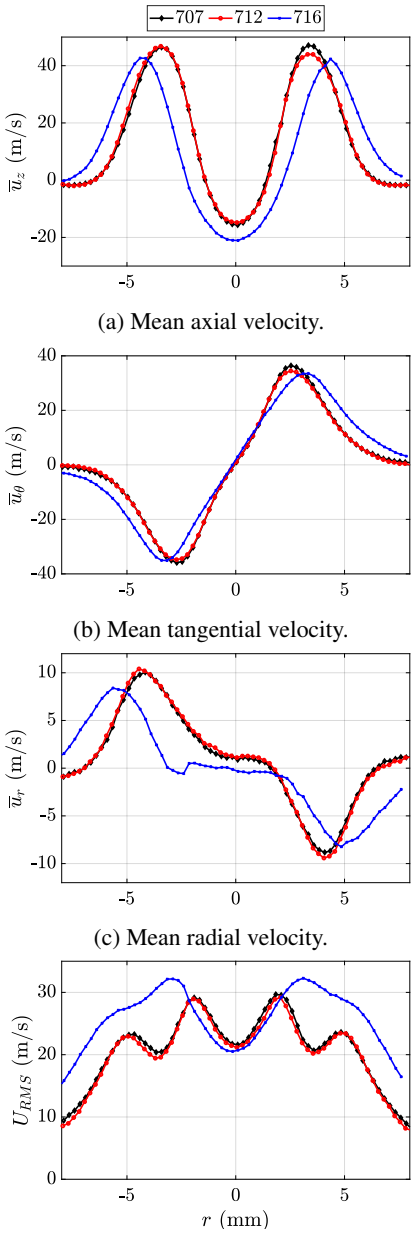

(a) Mean axial velocity.

(b) Mean tangential velocity.

(c) Mean radial velocity.

(d) Mean turbulent velocity.

Fig. 2: Mean air flow velocity profiles measured 5 mm downstream of the dump plane for three injection systems (see Tab. 1).

Table 1: Dimensions and main aerodynamic characteristics of the three swirlers with an air mass flow rate of 2.3 g s^{-1}. See Fig. 1 for the definition of dimensions d_{th} and R_0.

Swirler	d_{th} (mm)	R_0 (mm)	ΔP (kPa)	$\mathcal{S}$	f_{PVC} (kHz)
707	4	4.6	2.79	0.62	3.95
712	3	2.28	3.45	0.6	3.44
716	3.5	4.7	4.4	0.78	3.47

but different head loss levels. Swirler 716 yields a significantly different flow pattern: due to the higher rotation rate, the angle of the air jet is wider, the level of turbulence and the recirculating velocities are higher, and the diameter of the recirculation zone is augmented. Experimental swirl numbers calculated at $z = 5$ mm using the conventional formula [25]

$$\mathcal{S} = \frac{\int_0^{2R_{inj}} \overline{U_\theta}\,\overline{U_x}\, r^2 dr}{R_{inj} \int_0^{2R_{inj}} \overline{U_x}^2\, r dr} \tag{1}$$

are quoted in Tab. 1. The dynamics of the Precessing Vortex Core (PVC) is also investigated in the absence of spray using a constant temperature hot wire anemometer (Dantec-Dynamics miniCTA with 55P16 probe). The frequency f_{PVC} of the $m = 1$ PVC (first order in azimuth, single helix PVC) is reported for all three swirlers in Tab. 1. Although the external, time-averaged aerodynamic profiles of swirlers 707 and 712 are quite similar, one observes that the frequency of the PVC is higher for swirler 707. The PVC frequency of swirler 716 is also close to that of swirler 712. However, this injection system features an intermittency between a first order ($m = 1$), single helix PVC, and a second order ($m = 2$), double helix PVC with a frequency twice that of the single helix PVC. Characterization of a double helix PVC in SICCA-Spray is presented using time-resolved particle tomography and LES in [26].

The circumferential spray droplet size distribution is determined by moving the laser probe volume of the PDA system on a cylindrical mesh. The Sauter mean droplet diameters d_{32} are displayed in polar coordinates in Fig. 3 by placing a symbol at a distance from the center corresponding to the d_{32} value. The plots correspond to three radii with respect to the injector axis. The patterns pertaining to the damaged atomizer AD and swirlers 707 and 712, are not axisymmetric. This is confirmed in the polar plots of the mean diameter d_{10} corresponding to the same injection systems and operating conditions (not shown here). The circumferential Sauter mean droplet diameter distribution pertaining to swirler 716, with the damaged atomizer AD, is more regular. When atomizer AG is employed, the circumferential pattern of the spray is much more homogeneous for all three swirlers. A slight asymmetry is still present with swirler 716 and atomizer AG and found to be quite reproducible. From these observations, one concludes that the damaged atomizer AD is mainly responsible for the skewed circumferential distribution, while an undamaged atomizer AG creates a fairly homogeneous spray. One also finds that an injector with a higher level of swirl interacts with the spray such that the droplet pattern is more robust to defects in the atomizer. It is however not possible to conclude at this point about the physical processes that homogenize the spray distribution or create the slight asymmetry with swirler 716. The internal aerodynamics of swirler 716 are probably conducive to a higher level of turbulent mixing. It appears indeed from velocity data measured downstream of the injector (Fig. 2) that the turbulent intensity is higher with this swirler compared to 707 and 712. An-

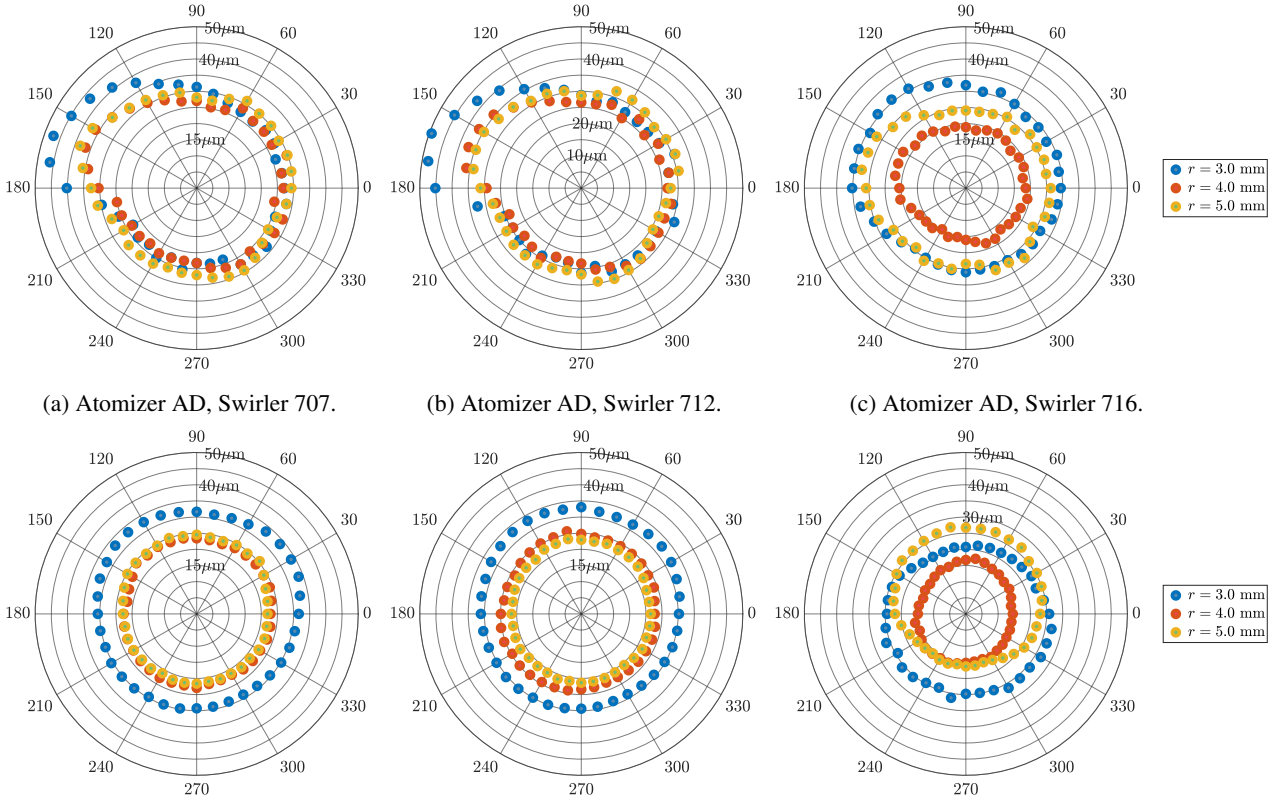

(a) Atomizer AD, Swirler 707. (b) Atomizer AD, Swirler 712. (c) Atomizer AD, Swirler 716.

(d) Atomizer AG, Swirler 707. (e) Atomizer AG, Swirler 712. (f) Atomizer AG, Swirler 716.

Fig. 3: Circumferential distribution of the Sauter mean droplet diameter d_{32}. For each data point the azimuthal angle on the graph corresponds to the azimuthal angle in the experiment, the color of the point to the radial coordinate of the measurement point, and the radial position in the graph corresponds to the value of d_{32} (the gray circles correspond to 5, 10, 15... µm as indicated in the graphs when this is possible). Measurements acquired at $z = 2.5\,\text{mm}$.

other possibility may be that the interaction between the flow and the conical liquid sheet formed at the tip of the atomizer plays a role in the azimuthal distribution of droplet sizes. The higher swirl number of swirler 716 is creating a stronger recirculation zone near the tip of the atomizer. These features may have a direct impact on the atomization process itself [4]. One reviewer also suggests that the PVC might be the cause of the asymmetry observed with swirler 716 and atomizer AG. Indeed, if the transition between the single and double helix PVC of this swirler happens preferentially at some azimuthal position, it may be the root of the deformed pattern that has been observed.

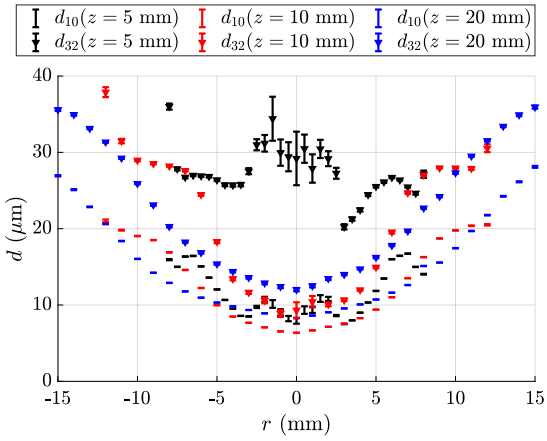

Fig. 4: Radial profiles of mean droplet diameter d_{10} and Sauter mean diameter d_{32} obtained at $z = 5$, 10 and 20 mm above the backplane (red dotted lines in Fig. 5). Swirler 707. Error bars indicate the 95% statistical confidence interval obtained from bootstrapping.

DETAILED EXPERIMENTAL CHARACTERIZATION OF THE FUEL SPRAY

The focus is now placed on the detailed analysis of PDA measurements obtained using atomizer AG and swirler 707. Figure 4 presents the mean (d_{10}) and Sauter mean (d_{32}) diameters at different distances from the injector dump plane. The droplet sizes appear relatively homogeneous across the radial dimension at $z = 5\,\text{mm}$. Typical values are then $d_{10} = 10\,\mu\text{m}$ and $d_{32} = 27\,\mu\text{m}$. Note that the mean diameters have a very high statistical uncertainty in a region around the injector axis ($r < 2.5\,\text{mm}$) as the number of droplets that travel in this region is quite low, as is well exemplified in the laser tomography image in Fig. 5. This is a common problem when computing Sauter mean diameter from PDA measurements

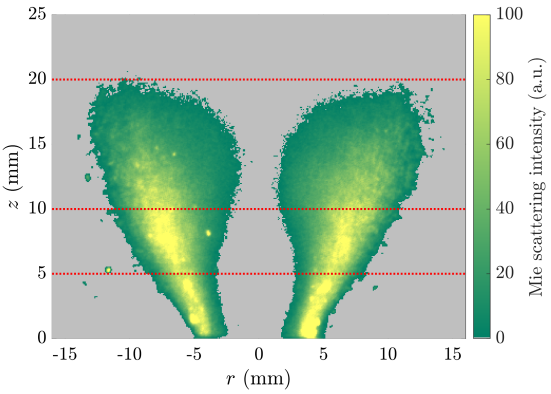

Fig. 5: Laser tomography of the spray above the dump plane, in the presence of flow. Swirler 707. Red dotted lines: PDA measurements heights.

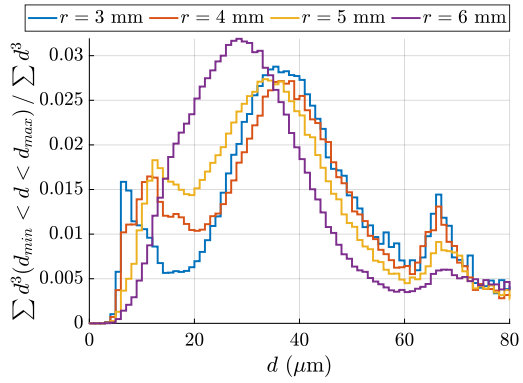

Fig. 6: Volumetric droplet size histograms measured at four radial positions $z = 5\,\text{mm}$ above the backplane. The plots correspond to the fraction of the total liquid volume for each droplet diameter class in the histogram.

as noted in [27]. In general, the droplet diameter profiles have a bowl shape with larger droplets on the outside, which is expected due to segregation based on the Stokes number in swirling flows [7, 8]. One may note however that the difference between the profiles of d_{10} and those of d_{32} decreases sharply with the distance from the backplane, indicating that an originally highly polydisperse distribution at $z = 5\,\text{mm}$ becomes nearly monodisperse at $z = 20\,\text{mm}$ and that this is probably due to a combination of swirl induced particle segregation and vaporisation. Finally, one may also note that in the tomographic image of Fig. 5, the signal is very intense near the backplane around $r = r_{inj} = 4\,\text{mm}$. It was observed in this system that a film of liquid droplets is formed on the conical convergent section of the injector, and that this film is being atomized in an air blast manner. Droplet size histograms are shown in Fig. 6 for different radial positions at $z = 5\,\text{mm}$. These positions correspond to areas where large numbers of droplets are present (see Fig. 5). The distributions are highly polydisperse, and essentially feature three peaks: the first, at approximately $d = 10 - 15\,\mu\text{m}$ appears small here in this volumic representation, but corresponds to the main peak of the droplet number distribution. The second is around $d = 30 - 40\,\mu\text{m}$ while the third represents a small number of relatively large droplets ($d \simeq 70\,\mu\text{m}$). One may suspect that these multiple peaks arise from the different atomization processes taking place in the experiment, and result: from the flow interacting with the atomizer spray; from the liquid film escaping from the conical convergent; and from air-blast by the swirling air flow in the injector endpiece.

To further analyze the spray characteristics, the distribution of axial velocity conditioned by the droplet diameter is shown in Fig. 7. For smaller droplets, the distribution is fairly wide and continuous, as could be expected as these droplets behave essentially like tracers in a highly turbulent flow. For larger droplets, the velocity distribution is much narrower with a sharp peak around $29\,\text{m}\,\text{s}^{-1}$. At $r = 5\,\text{mm}$, a second peak seems to be present at a much lower velocity for larger droplets. This is confirmed by the velocity histograms in red in Fig. 8. These velocity histograms pertain to droplets with a diameter larger than $45\,\mu\text{m}$. At $r = 4\,\text{mm}$ the histograms exhibit a single peak around $29\,\text{m}\,\text{s}^{-1}$. At $r = 5$ and $r = 6\,\text{mm}$ the distribution becomes bimodal with a second peak at a much lower velocity. The velocity statistics for the air flow at the same positions are shown in black alongside those of larger droplets in Fig. 8. These histograms feature a single very wide peak at a velocity that notably differs from that of the large fuel droplets.

Such a bimodal velocity distribution for large droplets is also identified by Wang et al. [29] in the injector from the CFM56 series of engines. This injector is a two-stage counterswirling design. Fuel is injected on the centerline in a hollow cone pattern and subsequently hits the wall of a venturi, forming a film. The authors attribute the bimodality of the velocity distribution to two possible and distinct droplet histories: those formed by the atomizer and those formed by the film have different velocities. Given that filming is also observed in the "SICCA-Spray" experiments, a similar explanation for the bimodality of the velocity distribution can be invoked here: some droplets directly originate from the atomizer while others are formed in the liquid fuel film located on the convergent section of the injector. However, in the present case, the highest velocity values correspond to the droplets from the atomizer. Indeed, using a simple mass and momentum balance on the atomizer, one concludes that droplets are injected with an axial velocity in the order of 30 to $50\,\text{m}\,\text{s}^{-1}$ and, given their large size, their velocity does not change much when they reach the measurement section. This will be confirmed and complemented with the large eddy simulations carried out in what follows.

LARGE EDDY SIMULATION OF THE GASEOUS AND DISPERSED PHASES

Euler-Lagrange numerical setup

The present simulations are carried out on the injector equipped with swirler 707, using the fully compressible, LES-filtered, Navier-Stokes solver AVBP jointly developed

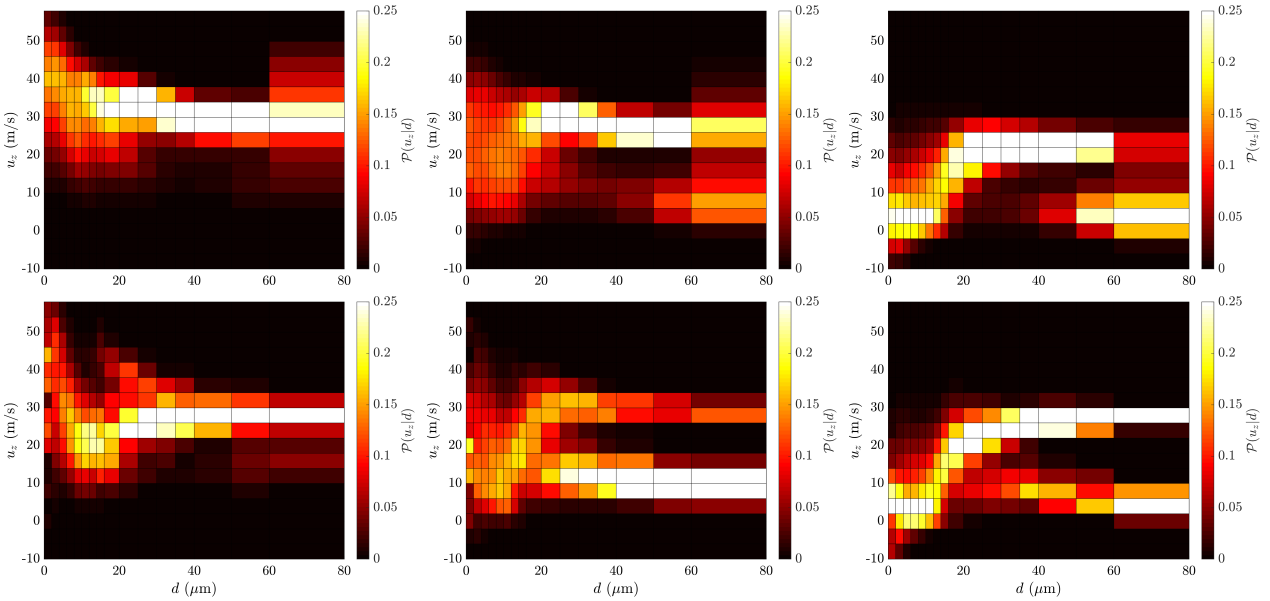

(a) $r = 4$ mm. (b) $r = 5$ mm. (c) $r = 6$ mm.

Fig. 7: Probability of axial velocity conditioned by the droplet diameter at $z = 5$ mm and at radial positions $r = 4$, 5 and 6 mm. On the top row, experimental results measured by PDA. On the bottom row, simulation (LES) results that will be discussed in the LES section. In both cases, circumferential averaging is performed.

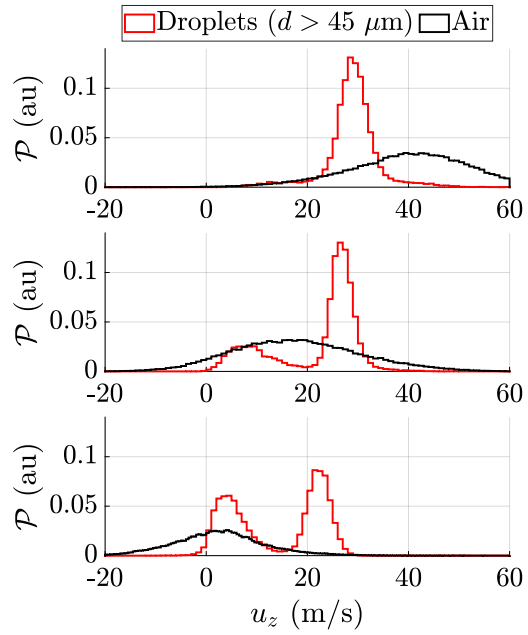

Fig. 8: In red, axial velocity histogram for large droplets (diameter greater than 45 µm) at 3 radial positions (from top to bottom, $r = 4$, 5 and 6 mm, all taken at $z = 5$ mm). In black, air axial velocity histogram from LDV measurements.

by CERFACS and IFPEN [30]. Three gaseous species (O_2, N_2 and C_7H_{16}) are transported under a unity Lewis assumption. Integration is based on TTGC, a third order in space and time numerical scheme [31], along with NSCBC boundary conditions [32]. Boundaries within the injection system are modeled using a logarithmic law of the wall. The impact of subgrid scales on the resolved momentum is accounted for using the SIGMA model [33].

The extent of the numerical domain is that of the schematic view in Fig. 1: the plenum is shortened, and the injector exhausts to an atmosphere with a slow coflow (1 m s^{-1}) added for stability. The mesh comprises 28 million tetrahedral elements. Starting from an initial, uniform mesh size in the injector ($\Delta x = 0.3$ mm), the automatic mesh refinement method proposed in [34] is used to reduce the cell sizes down to $\Delta x \simeq 60$ µm. Validation of gaseous phase velocity profiles is performed on the purely gaseous computation without droplet injection. Numerical results are compared to LDV measurements in Fig. 9 showing a very good agreement for the three velocity components and the velocity fluctuations.

The dynamics of the disperse liquid phase is represented with a Lagrangian formalism. The Schiller-Naumann correlation [35] is used to compute the drag force on the particles. Evaporation is estimated using the model proposed by Abramzon and Sirignano [36] with a constant value for Prandtl and Schmidt numbers: $Pr = 0.976$ and $Sc = 1.343$ [37]. Dependence of evaporation on the droplet Reynolds number uses a Frossling correlation. Two-way coupling between the disperse and gaseous phase is taken into account using a second order linear interpolation. Gravity and shear effects are considered negligible compared to drag and the time integration for the trajectories uses a two-step Runge-Kutta scheme.

Particle-wall interaction is a critical aspect in this simulation, because some of the droplets hit the wall of the coni-

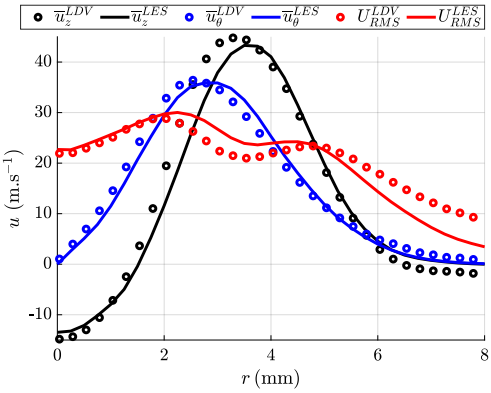

Fig. 9: Comparison between LES velocity profiles and LDV measurements at $z = 5\,\text{mm}$. The plots show mean axial and tangential velocities as well as overall RMS velocity.

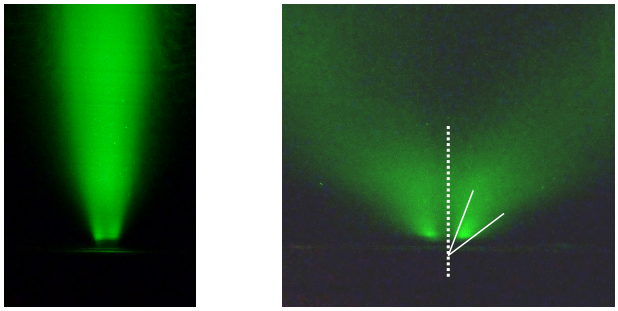

(a) $\dot{m}_{air} = 0$ (b) $\dot{m}_{air} = 2.3\,\text{g}\,\text{s}^{-1}$

Fig. 10: Tomographic visualization of the spray at the tip of the atomizer. The spray is illuminated by a laser sheet just above the outlet of the atomizer. In this experiment, the end plate of the atomizer (golden disc in Fig. 1(c)) is removed to gain optical access. The laser sheet crosses the atomizer on its centerline, and the spray image is obtained with a long exposure time. Left image : fuel injection without air flow. Right image : with air flow.

cal end piece. Particles may splash on the wall, rebound, slip in an isolated manner or form a film. This simulation uses the film model proposed by Chaussonnet et al. [38]. This model imposes the velocity of particles close to the wall as a group based on the solution of a set of Saint Venant Eulerian equations for film thickness and momentum.

Liquid injection model

A critical aspect of spray simulations in a Lagrangian framework is the specification of the initial position, size and velocity distributions for the particles. There are various models in the literature that describe pressure-swirl atomizers such as the FIMUR model [39]. However these models do not yield velocity distributions that are consistent with what is known from the present measurements. Indeed, it can be experimentally observed, as shown in Fig. 10, that the atomizer and the air flow interact, leading to a drastic change in injection properties when air flow is present. Such drastic changes in the near atomizer flow field caused by addition of a swirling air flow addition are also reported in the literature: the term "explosive breakup" is coined for this phenomenon by Hopfinger & Lasheras [40], who studied a round water jet in a swirling air flow. Above a certain critical value of the swirl number, the plain jet underwent a violent radial expansion, forming a hollow cone and dramatically improving atomization. In [41], the authors analyze the spray formed by a simplex atomizer in a swirling air flow, and observe a transition similar to that of Fig. 10 from a closed spray to a hollow cone as air flow is increased. They observe that this transition is affected by a strong hysteresis. Thus, a dynamical injection model accounting for coupling with the air flow would be required. This is not attempted in the present simulations and a simpler uncoupled model is adopted in which the initial spray characteristics are adjusted by making use of experimental data obtained in the injector near field. Four main parameters must be determined: the position of fuel injection, the initial droplet size distribution, their velocity and injection angle.

The initial droplets are injected on a ring of inner radius 27 µm and outer radius 54 µm. The droplet size distribution is the one measured at $z = 5\,\text{mm}$. This choice is driven by two reasons. First, there is at present no accurate model for the determination of droplet size distribution at the atomizer's exit, and there is no direct optical access to perform in situ experimental measurements. Second, several physical phenomena (secondary atomization, splashing, droplet-droplet interactions) are not accounted for in the simulation because of the lack of fully predictive models. By imposing the experimental distribution, one circumvents these issues, making the assumption that the corresponding physical processes only take place in the immediate vicinity of the atomizer and are characterized by short time scales. Simulations with diameter distributions from measurements at several different radial positions as input were performed, but using a droplet diameter PDF averaged over all experimentally available radial positions gave the best results. The injected distribution is corrected for evaporation between the atomizer and the PDA measurement section assuming that it follows a d^2 law. This correction is important for the smaller droplets, for which this simplistic evaporation law is acceptable as they behave as tracers in an isothermal flow [3]. For this correction, a constant value of the d^2 law coefficient $\lambda_{d2} = 1.65 \times 10^{-8}\ \text{m}^2\,\text{s}^{-1}$ given by [42] is used. The time of flight of particles from the atomizer to the measurement point is estimated using LES. The histogram of the corrected distribution is shown in Fig. 11. One may observe that droplets initially smaller than approximately 5 µm are fully evaporated and cannot be recovered. In practice, this has a negligible impact as these droplets represent a small fraction of the total injected mass, and this will not bias the comparison between experiment and LES at the PDA measurement section. One side advantage is that the tracking of these droplets would have induced a high CPU cost.

To determine the axial injection velocity by taking advantage of experimental data, it is instructive to examine

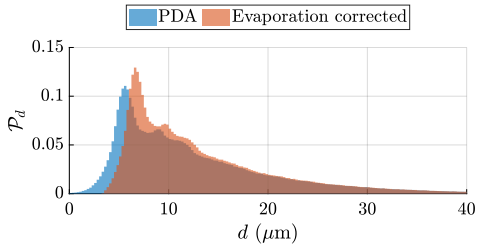

Fig. 11: Measured (blue) and injected (brown) droplet distribution. The injected distribution is corrected for evaporation.

the dynamics of large droplets. Using a simplified model for the droplet dynamics, only accounting for viscous drag following Stokes' law, the velocity $\mathbf{u_d}$ of a droplet of diameter d in an air flow at velocity $\mathbf{u}$ is given by $\dot{\mathbf{u}}_\mathbf{d} = [\mathbf{u}-\mathbf{u_d}]/\tau_d$ where $\tau_d = \left(\rho_l d^2\right)/(18\mu)$ is a characteristic time for the droplet acceleration, with ρ_l the density of the liquid, d the diameter of the droplet, and μ the viscosity of air. For a given time of flight in a uniform air flow with velocity $\overline{U}_{air}$, an upper bound for this velocity change for a particle injected with the velocity $\overline{U}_{p,0}$ can be estimated from: $\delta\overline{U} \simeq \left(\overline{U}_{air}-\overline{U}_{p,0}\right)\left[1-\exp\left(-St^{-1}\right)\right]$ where St is the Stokes number based on the particle time of flight, $St = \tau_d/\tau_{flight}$. For an upper bound of the air flow velocity $\overline{U}_{air} = 70\,\mathrm{m\,s^{-1}}$ and a flight time corresponding to the time taken by the largest particles ($d > 50\,\mu$m) to travel from the atomizer to the PDA measurement volume, the increase in axial velocity for such a particle is less than $3\,\mathrm{m\,s^{-1}}$. Thus, the velocity of the larger droplets is roughly the same as their injection velocity. It is then reasonable to assign an initial value $29\,\mathrm{m\,s^{-1}}$ to all the initial droplets.

The injection angle of each droplet is randomly chosen by normally distributing its values with a mean θ_0 and a standard deviation $\delta\theta$. Initial values for these parameters are deduced from the tomographic images of the spray with air flow (Fig. 10). A parametric study of several LES is then conducted by varying θ_0 and $\delta\theta$ around these initial values to find the optimal set of parameters, $\theta_0 = 37\,\mathrm{deg}$ and $\delta\theta = 8\,\mathrm{deg}$.

Validation of the simulation

Volumetric cumulative distribution function of droplet diameter are compared between LES and PDA measurements at two locations in Fig. 12. At $r = 5\,\mathrm{mm}$, the agreement is excellent. At $r = 4\,\mathrm{mm}$, the proportion of large droplets is overpredicted by about 20% by volume. Mean and Sauter mean diameters are compared with PDA measurements in Fig. 13. The agreement is fairly good, especially in the regions characterized by higher liquid volume flux that are of higher practical interest. Some discrepancies are observed in the inner recirculation region at $z = 5\,\mathrm{mm}$. This could be expected as the number of droplets in this region is very low, also leading to high statistical uncertainties. Overprediction of d_{32} around $r = 4\,\mathrm{mm}$ are mainly due to the film model and this topic is discussed in Appendix A.

The probabilities of axial velocity conditioned by the

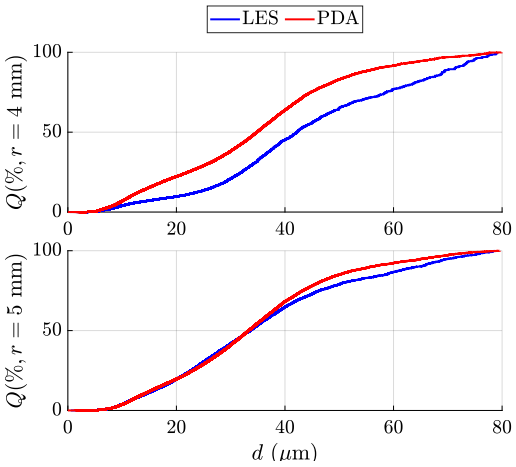

Fig. 12: LES and PDA volumetric cumulative distribution function of droplet sizes at $r = 4$ (top) and $r = 5\,\mathrm{mm}$ (bottom). $z = 5\,\mathrm{mm}$.

droplet diameter are gathered in Fig. 7 for the points located at r= 4, 5 and 6 mm and at 5 mm from the outlet. The bimodality of the velocity distribution for large droplets observed experimentally at $r = 5\,\mathrm{mm}$ is retrieved albeit overestimated. As is seen experimentally, this bimodality is also not observed at $r = 4\,\mathrm{mm}$. The agreement between LES and experimental measurements is also excellent at $r = 6\,\mathrm{mm}$. The locations of the velocity peaks are also well retrieved for all positions and for both peaks.

Discussion

Backward-forward Lagrangian particle tracking is employed in Fig. 14 to examine droplet histories from the LES data. Only droplets larger than $d > 40\,\mu\mathrm{m}$ are considered. The following process is used. Droplet trajectories are projected to the (rz) plane. All droplets that pass in the vicinity of the control volume (0.5 mm diameter torus around the point of interest at $r = 5\,\mathrm{mm}, z = 5\,\mathrm{mm}$) are then extracted. In this manner, the history of droplets whose behavior is examined in the center image of Fig. 7 can be analyzed.

Figure 14(a) presents the trajectories of all 516 large particles observed to come in the vicinity of $(r,z) = (5,5)$ mm during 5 ms of simulation, along with the geometry of the injector (in black). Two populations can be distinguished. Some droplets hit the conical convergent wall of the injector, others do not, and those two groups are well separated. The dynamics of 20 particles that do not collide with the wall is examined in more details in Fig. 14(b). Their axial velocity at every point in the trajectory is shown by their color. These particles have a high initial axial momentum communicated at injection. They are slightly accelerated after the outlet of the injector and reach velocities of the order of $30\,\mathrm{m\,s^{-1}}$ in the vicinity of the point of interest $(r,z) = (5,5)$ mm. Those particles stay closely together over a long distance.

Figure 14(c) is focused on particles that have formed a film on the convergent section. As they hit the wall at a close to normal angle, their initial momentum is mostly dissipated

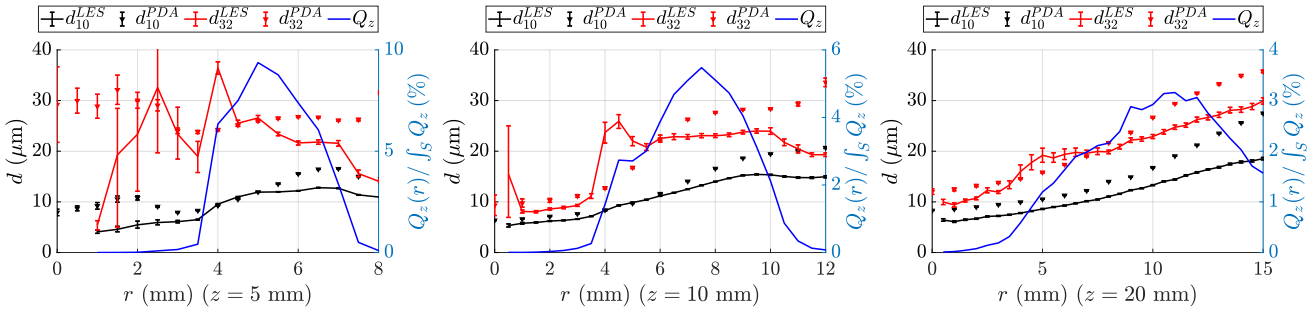

Fig. 13: Comparison of mean (black) and Sauter mean (red) diameters from the LES with PDA measurements. Three measurement sections are considered ($z = 5$, 10 and 20 mm). Azimuthal averages are performed in both cases. On the right axis, the radial distribution of the axial liquid volume flux is shown as a blue solid line.

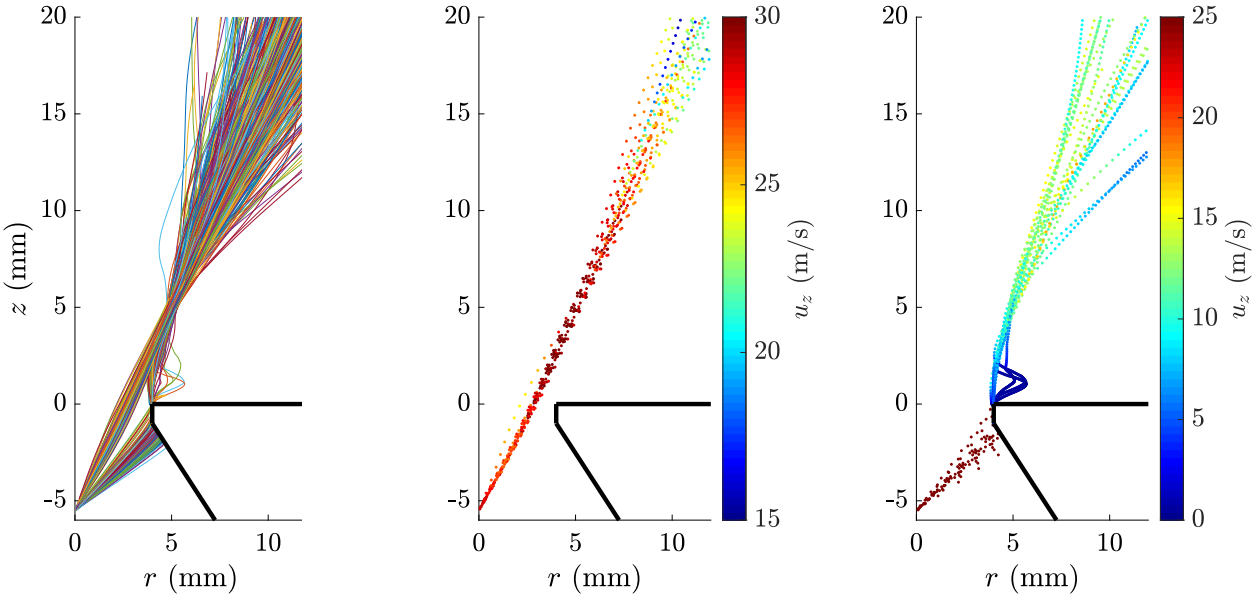

(a) All particles.

(b) 20 particles not hitting the wall.

(c) 20 particles hitting the wall.

Fig. 14: Backward - forward Lagrangian particle tracking of all droplets that pass inside the control volume (0.5 mm diameter torus around the point of interest at $r = 5\,\text{mm}, z = 5\,\text{mm}$). In black, geometry of the upper part of the injector. On the right, trajectories are colored by axial velocity.

at this point. They are released at the edge ($(r,z) = (5,5)$) with a lower velocity of the order of $10\,\text{m}\,\text{s}^{-1}$ and subsequently accelerated by the flow.

Additional materials to this paper present experimental measurements that have been performed on the spray formed when using injector 712 at the same operating point. Results and conclusion are similar to those obtained with swirler 707. The same characterization is also presented for swirler 716 at a slightly differing operating point corresponding to Flame Describing Function measurements in [28]. The fuel flow rate is nearly identical to that used for the present characterization of swirlers 707 and 712, but the air flow rate is 15% higher. Similar features, and in particular the bimodality of the velocity distribution are also found. However, the probability of slower velocities is much higher with swirler 716. This may be caused by a wider spray angle which is observed on laser illumination in the near field of the atomizer.

CONCLUSION

This investigation is concerned with issues of technical importance in the engineering of swirling injectors for jet engine applications. The study is carried out on a laboratory scale injector designed to emulate a small helicopter engine injector. This unit features a pressure swirl simplex atomizer creating a hollow cone shaped spray of heptane droplets. The geometry is such that some of the droplets in the spray hit the injector end piece inner surface forming a liquid film. Using an experimental characterization of the spray in the form of polar plots, it is shown that asymmetries in the spray can be identified, and that these features are linked to manufacturing variability or in the present case to a damaged atomizer. Tests with swirlers having different levels of rate of rotation indicate that injector flows characterized by a higher swirl number tend to smooth out irregularities in the spray pattern. A second item of considerable importance in the numerical

simulation of liquid spray injectors is that of size and velocity distribution of the droplets. It is shown that suitable choices of the size and velocity distributions imposed in the atomizer near field are needed to obtain a good match between experimental data and results of simulations. The injected distributions are derived by optimizing the input set of parameters determined from laser tomographic visualizations of the spray and Phase Doppler Anemometry. This allows high fidelity LES simulations of the spray. It is shown in particular that an experimentally observed bimodality in the velocity distribution for large droplets is retrieved and that this feature can be linked to the droplet histories. Droplets forming the liquid film are slowed down and form a second, low velocity peak in the distribution. It is worth noting that the bimodal character of the velocity distribution in the spray of aeronautical injection systems was observed some time ago by McDonnell et al. [9], and that their interpretation is validated by the present work.

Acknowledgements

This work benefited from the support of SafranTech (contract NF5Z-5100), and of project FASMIC ANR-16-CE22-0013 of the French National Research Agency (ANR). This work was granted access to the HPC resources of CINES under the allocation 2019-A0072B10315 attributed by GENCI. The authors wish to thank J.M. Dupays, E. Lo Schiavo, D. Laera and L.Y.M. Gicquel for their help in the use of AVBP and the film model boundary condition.

References

[1] Lefebvre, A. H., 1995. "The role of fuel preparation in low-emission combustion". *J. Eng. Gas Turb. Power,* ***117***(4), pp. 617–654.

[2] Lefebvre, A. H., and Ballal, D. R., 2010. *Gas turbine combustion : alternative fuels and emissions*. Taylor & Francis.

[3] Lefebvre, A. H., 1989. *Atomization and Sprays*. Taylor & Francis.

[4] Rajamanickam, K., and Basu, S., 2017. "Insights into the dynamics of spray-swirl interactions". *J. Fluid Mech.,* ***810***, jan, pp. 82–126.

[5] Sharma, S., Ghate, K., Sundararajan, T., and Sahu, S., 2019. "Effects of air swirler geometry on air and spray droplet interactions in a spray chamber". *Adv. Mech. Eng.,* ***11***(5), may, p. 168781401985097.

[6] Hardalupas, Y., Taylor, A. M. K. P., and Whitelaw, J. H., 1992. "Particle Dispersion in a Vertical round Sudden-Expansion Flow". *Philos. Trans. R. Soc. A,* ***341***(1662), dec, pp. 411–442.

[7] Dring, R. P., and Suo, M., 1978. "Particle trajectories in swirling flows". *J. Energy,* ***2***(4), pp. 232–237.

[8] Kriebel, A. R., 1961. "Particle Trajectories in a Gas Centrifuge". *Journal of Basic Engineering,* ***83***(3), p. 333.

[9] McDonnell, V. G., Cameron, C. D., and Samuelsen, G. S., 1990. "Symmetry assessment of an air-blast atomizer spray". *J. Propul. Power,* ***6***(4), jul, pp. 375–381.

[10] Lecourt, R., Linassier, G., and Lavergne, G., 2011. "Detailed characterisation of a swirled air/kerosene spray in reactive and non-reactive conditions downstream from an actual turbojet injection system". In Proc. ASME TurboExpo.

[11] Jaegle, F., Senoner, J.-M., García, M., Bismes, F., Lecourt, R., Cuenot, B., and Poinsot, T., 2011. "Eulerian and Lagrangian spray simulations of an aeronautical multipoint injector". *Proc. Combust. Inst.,* ***33***(2), jan, pp. 2099–2107.

[12] Guedot, L., Lartigue, G., and Moureau, V., 2018. "Modeling and Analysis of the Interactions of Coherent Structures with a Spray Flame in a Swirl Burner". Springer, Cham, pp. 15–26.

[13] Franzelli, B., Vié, A., Fiorina, B., and Darabiha, N., 2013. "Large Eddy Simulation of Swirling Kerosene/Air Spray Flame Using Tabulated Chemistry". In Proc. ASME TurboExpo.

[14] Renaud, A., Ducruix, S., and Zimmer, L., 2019. "Experimental Study of the Precessing Vortex Core Impact on the Liquid Fuel Spray in a Gas Turbine Model Combustor". *J. Eng. Gas Turb. Power,* ***141***(11), nov.

[15] Keller, J., Gebretsadik, M., Habisreuther, P., Turrini, F., Zarzalis, N., and Trimis, D., 2015. "Numerical and experimental investigation on droplet dynamics and dispersion of a jet engine injector". *Int. J. Multiph. Flow,* ***75***, oct, pp. 144–162.

[16] Gajan, P., Strzelecki, A., Platet, B., Lecourt, R., and Giuliani, F., 2007. "Investigation of Spray Behavior Downstream of an Aeroengine Injector with Acoustic Excitation". *J. Propul. Power,* ***23***(2), mar, pp. 390–397.

[17] Kim, W., Zhang, S., Palies, P., Cohen, J., Liljenberg, S., and Hautman, D., 2012. "The behavior of liquid fuel sprays in acoustically-forced air swirler flows". In Proc. ASME TurboExpo.

[18] Eckstein, J., Freitag, E., Hirsch, C., and Sattelmayer, T., 2006. "Experimental study on the role of entropy waves in low-frequency oscillations in a RQL combustor". *J. Eng. Gas Turb. Power,* ***128***(2), apr, pp. 264–270.

[19] Tachibana, S., Saito, K., Yamamoto, T., Makida, M., Kitano, T., and Kurose, R., 2015. "Experimental and numerical investigation of thermo-acoustic instability in a liquid-fuel aero-engine combustor at elevated pressure: Validity of large-eddy simulation of spray combustion". *Combust. Flame,* ***162***(6), jun, pp. 2621–2637.

[20] Lee, J.-Y., Lubarsky, E., and Zinn, B. T., 2005. ""Slow" active control of combustion instabilities by modification of liquid fuel spray properties". *Proc. Combust. Inst.,* ***30***(2), jan, pp. 1757–1764.

[21] Vignat, G., Durox, D., Prieur, K., and Candel, S., 2019. "An experimental study into the effect of injector pressure loss on self-sustained combustion instabilities in a swirled spray burner". *Proc. Combust. Inst.,* ***37***(4).

[22] Vignat, G., Durox, D., Renaud, A., and Candel, S.,

2020. “High Amplitude Combustion Instabilities in an Annular Combustor Inducing Pressure Field Deformation and Flame Blow Off”. *J. Eng. Gas Turb. Power,* ***142***(1), jan, p. 011016.

[23] Prieur, K., Durox, D., Beaunier, J., Schuller, T., and Candel, S., 2017. “Ignition dynamics in an annular combustor for liquid spray and premixed gaseous injection”. *Proc. Combust. Inst.,* ***36***(3), pp. 3717–3724.

[24] Durox, D., Ducruix, S., and Lacas, F., 1999. “Flow seeding with an air nebulizer”. *Exp. Fluids,* ***27***(5), oct, pp. 408–413.

[25] Beer, J. M., and Chigier, N. A., 1972. *Combustion aerodynamics*.

[26] Vignat, G., Durox, D., Prieur, K., Lancien, T., Vicquelin, R., and Candel, S., 2018. “Tomographie à très haute cadence de flammes turbulentes swirlées au moyen du dioxyde d’étain”. In 16ème Congrès Francophone de Techniques Laser pour la mécanique des fluides, Sept. 2018, Dourdan.

[27] McDonnell, V. G., Samuelsen, G. S., Wang, M. R., Hong, C. H., and Lai, W. H., 1994. “Interlaboratory comparison of phase Doppler measurements in a research simplex atomizer spray”. *J. Propul. Power,* ***10***(3), may, pp. 402–409.

[28] Prieur, K., Durox, D., Vignat, G., Schuller, T., and Candel, S., 2017. “Experimental determinations of Flame Describing Functions of swirling spray flames”. In Colloque INCA.

[29] Wang, H., McDonell, V. G., Sowa, W. A., and Samuelsen, S., 1994. “Experimental Study of a Model Gas Turbine Combustor Swirl Cup, Part 11: Droplet Dynamics”. *J. Propul. Power,* ***10***(4), jul, pp. 446–452.

[30] http://www.cerfacs.fr/avbp7x/.

[31] Colin, O., and Rudgyard, M., 2000. “Development of High-Order Taylor–Galerkin Schemes for LES”. *J. Comput. Phys.,* ***162***(2), aug, pp. 338–371.

[32] Poinsot, T., and Lele, S., 1992. “Boundary conditions for direct simulations of compressible viscous flows”. *J. Comput. Phys.,* ***101***(1), jul, pp. 104–129.

[33] Baya Toda, H., Cabrit, O., Balarac, G., Bose, S., Lee, J., Choi A N, H., and Nicoud, F., 2010. “A subgrid-scale model based on singular values for LES in complex geometries”. In Center for Turbulence Research Proceedings of the Summer Program.

[34] Daviller, G., Brebion, M., Xavier, P., Staffelbach, G., Müller, J.-D., and Poinsot, T., 2017. “A Mesh Adaptation Strategy to Predict Pressure Losses in LES of Swirled Flows”. *Flow Turbul. Combust.,* ***99***(1), jul, pp. 93–118.

[35] Schiller, L., and Naumann, A., 1935. “A Drag Coefficient Correlation”. *Zeitschrift des Vereins Deutscher Ingenieure,* ***77***, pp. 318–320.

[36] Abramzon, B., and Sirignano, W. A., 1989. “Droplet vaporization model for spray combustion calculations”. *Int. J. Heat Mass Transf.,* ***32***(9), pp. 1605–1618.

[37] Sanchez, P. S., 2012. “Modeling the dispersion and evaporation of sprays in aeronautical combustion chambers”. PhD thesis, Université de Toulouse, jan.

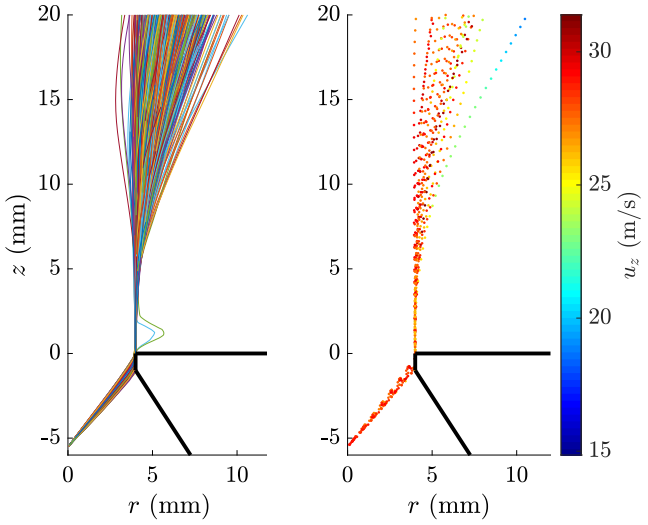

(a) All particles. (b) 20 particles hitting the wall.

Fig. 15: Backward - forward lagrangian particle tracking of all droplets that pass inside the control volume (0.5 mm diameter torus around the point of interest at $r = 4\,\text{mm}, z = 5\,\text{mm}$). On the right, trajectories are colored by axial velocity.

[38] Chaussonnet, G., Riber, E., Vermorel, O., Cuenot, B., Gepperth, S., and Koch, R., 2013. “Large Eddy Simulation of a prefilming airblast atomizer”. In ILASS, 25th European Conference on Liquid Atomization and Spray Systems, Chania, Greece, 1-4 September 2013.

[39] Sanjosé, M., Senoner, J., Jaegle, F., Cuenot, B., Moreau, S., and Poinsot, T., 2011. “Fuel injection model for Euler–Euler and Euler–Lagrange large-eddy simulations of an evaporating spray inside an aeronautical combustor”. *Int. J. Multiph. Flow,* ***37***(5), jun, pp. 514–529.

[40] Hopfinger, E. J., and Lasheras, J. C., 1996. “Explosive breakup of a liquid jet by a swirling coaxial gas jet”. *Phys. Fluids,* ***8***(7), pp. 1696–1698.

[41] Muthuselvan, G., Ghate, K. D., Rao, M. S., Iyengar, V. S., Thirumalachari, S., and Kothandaraman, S., 2018. “Experimental study of spray breakup phenomena in small-scale simplex atomizers with andwithout air swirl”. *At. Sprays,* ***28***(4), pp. 299–320.

[42] Chauveau, C., Birouk, M., Halter, F., and Gökalp, I., 2019. “An analysis of the droplet support fiber effect on the evaporation process”. *Int. J. Heat Mass Transf.,* ***128***, jan, pp. 885–891.

APPENDIX A. SPRAY PREDICTION AT THE INJECTOR OUTLET

It is interesting to examine the nearfield of the injector outlet. In this region and more specifically around $r = 4\,\text{mm}$, Fig. 13 indicates that the calculated d_{32} is over-predicted. This can be understood by examining the backward-forward lagrangian tracking displayed in Fig. 15 for particles pass-

ing around $r = 4\,\text{mm}, z = 5\,\text{mm}$ corresponding to the injector outlet. Large particles with high Stokes numbers observed at this position originate from the film boundary condition and have joined the film by hitting the small vertical wall found at the end of the conical convergent. These large particles conserve a high level of axial momentum that leads to clustering around $r = 4\,\text{mm}$ further downstream, while smaller particles will disperse more readily. In the experiment, the 90° corner is not sharp, but presents a small, non uniform chamfer due to the manufacturing process. If a more realistic, ragged edge geometry were adopted for this corner, a more realistic dispersion of the large particles would be achieved by the film model. A secondary edge atomization model would also be useful in this respect, but would require an improved knowledge of the spray at injection. This clustering effect probably also plays a role in the underestimation of the diameters in the outer flow region.